Surface Reconstruction of Halide Perovskites during Post-treatment

Shaun Tan,[1,2,‡] Tianyi Huang,[1,2,‡] Ilhan Yavuz,[3,‡] Rui Wang,[1] Marc H. Weber,[4] Yepin Zhao,[1] Maged Abdelsamie,[5] Michael E. Liao,[1] Hao-Cheng Wang,[6] Kenny Huynh,[1] Kung-Hwa Wei,[6] Jingjing Xue,[1] Finn Babbe,[2] Mark S. Goorsky,[1] Jin-Wook Lee,[7,*] Carolin M. Sutter-Fella,[2,8,*] and Yang Yang[1,*]

[1]Department of Materials Science and Engineering and California NanoSystems Institute, University of California Los Angeles, Los Angeles, California 90095, United States.

[2]Chemical Sciences Division, Lawrence Berkeley National Laboratory, Berkeley, California 94720, United States.

[3]Department of Physics, Marmara University, 34722, Ziverbey, Istanbul, Turkey.

[4]Center for Materials Research, Washington State University, Pullman, WA 99164, United States.

[5]Materials Science Division, Lawrence Berkeley National Laboratory, Berkeley, California 94720, United States.

[6]Department of Materials Science and Engineering, National Yang Ming Chiao Tung University, Hsinchu 30010, Taiwan

[7]SKKU Advanced Institute of Nanotechnology (SAINT) and Department of Nanoengineering, Sungkyunkwan University, Suwon 16419, Republic of Korea.

[8]Molecular Foundry, Lawrence Berkeley National Laboratory, Berkeley, California 94720, United States.

‡These authors contributed equally to this work.

***Correspondence to:**

Y. Yang, email: yangy@ucla.edu

C. M. Sutter-Fella, email: csutterfella@lbl.gov

J.-W. Lee, email: jw.lee@skku.edu

ABSTRACT

Post-fabrication surface treatment strategies have been instrumental to the stability and performance improvements of halide perovskite photovoltaics in recent years. However, consensus understanding of the complex reconstruction processes occurring at the surface is still lacking. Here, we combined complementary surface-sensitive and depth-resolved techniques to investigate the mechanistic reconstruction of the perovskite surface at the microscale level. We observed a reconstruction towards a more PbI_2-rich top surface induced by the commonly used solvent isopropyl alcohol (IPA). We discuss several implications of this reconstruction on the surface thermodynamics and energetics. Particularly, our observations suggest that IPA assists in the adsorption process of organic ammonium salts to the surface to enhance their defect passivation effects.

The record performance of single-junction halide perovskite solar cells (PSCs) have now exceeded 25 %.[1] Important breakthroughs on defect passivation strategies have contributed to the rapid performance improvements in recent years.[2,3] However, achievable voltage losses are still short of the theoretical limit. More importantly, it has become apparent that the migration and redistribution of charged point defects by a potential gradient is known to underly the operational instability of PSCs,[4–6] and this remains one of the major challenges of perovskite photovoltaics.

It has been reported that defect states causing non-radiative losses are dominantly located towards the top surface of halide perovskites.[7,8] This has motivated the development of surface passivation strategies by post-treatment of the perovskite film surface.[9] However, understanding of the complex reconstruction processes that can occur during the surface treatment procedures and any resulting changes to the interfacial charge dynamics are still lacking. This is urgently needed for targeted surface treatment strategies to minimize trial-and-error approaches. For this purpose, *in situ* spectroscopy is suited to monitor occurring changes on relevant time and length scales.[10–13]

In this study, we investigate the mechanistic reconstruction processes occurring at the perovskite surface during post-fabrication treatments. Through complementary surface-sensitive techniques, we observed the generation of defects and a reconstruction towards a more PbI_2-rich surface as isopropyl alcohol (IPA) is spun onto the surface. We show that this reconstruction has important implications on the thermodynamics and energetics of the perovskite surface. Importantly, our observations suggest that IPA assists in the anchoring process of organic ammonium salts to the perovskite surface.

IPA is ubiquitously used as the solvent to dissolve organic ammoniums for surface treatments, but formamidinium iodide (FAI), itself with the amidinium functional group, is also soluble in IPA. It is unclear what effects (if any) IPA has on the perovskite surface, given the short exposure timescales (~ms) at high rotation speeds (>4000 rpm). Conflicting results on the macroscopic bulk device/film properties have been reported. Beneficial improvements to film crystallinity, charge carrier dynamics, morphology, and device performance have been observed,[14,15] while detrimental effects to device stability were also reported.[16] To rationalize these contradictory results, we first attempted to explore the microscale phenomena occurring at the surface. Significantly, IPA remains perhaps a crucial solvent for post-treatment, since the most common surface passivating agents, such as phenylethylammonium iodide (PEAI) and octylammonium iodide (OAI), are essentially insoluble in low polarity solvents such as chloroform (CF) (**Figure S1**).

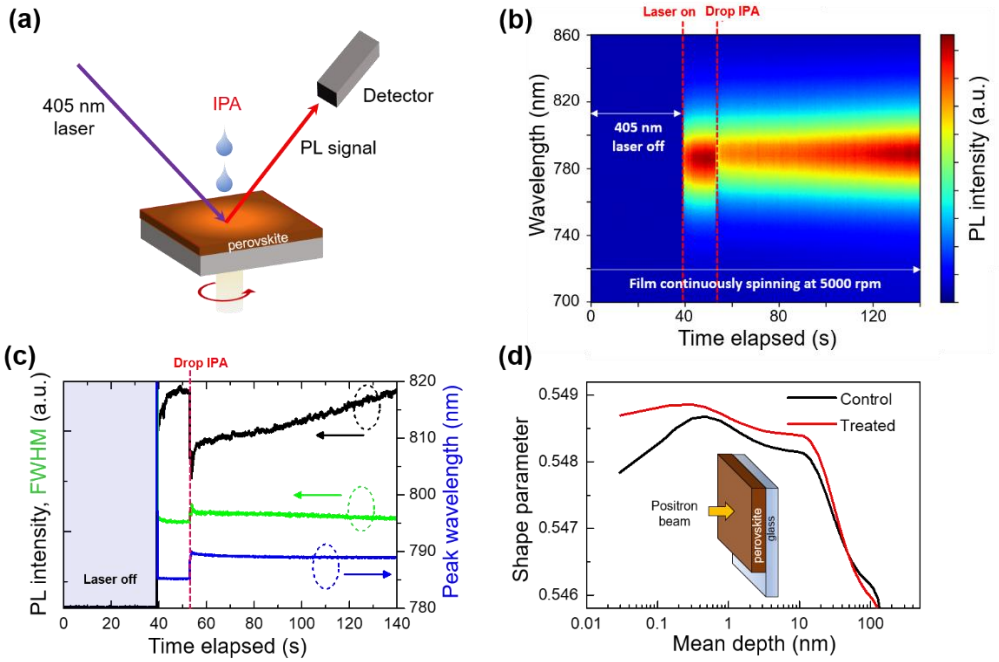

Figure 1. Defect generation by IPA treatment. (a) Schematic of the *in situ* PL measurement during IPA post-treatment. (b) *In situ* PL contour plot of a perovskite film undergoing surface treatment with IPA dropped at around 53 s. (c) Evolution of the PL parameters extracted from fitting (b). (d) PAS depth-profiling of the perovskite films.

The control perovskite is based on a $FAPbI_3$ composition with 5 mol% of added $MAPbBr_3$ fabricated by a one-step antisolvent quenching method. We monitored the photoluminescence (PL) of an as-fabricated perovskite film *in situ* with a 405 nm excitation wavelength (**Figure 1a**) in a nitrogen glovebox (<0.5 ppm O_2/H_2O). The laser penetration depth was estimated to be ~50 nm (**Figure S2**), and therefore sensitive to any potential changes in the surface charge carrier recombination behavior. The PL intensity abruptly decreased (23 % decrease) with a broadening and redshifting of the PL peak upon dropping IPA (**Figure 1b, 1c, Figure S3a**). In general, this is indicative of increased nonradiative carrier recombination, which implies the generation of charge-trapping defect states. Time-resolved PL (**Figure S3b**) of the perovskite films further support this, where the carrier lifetime fitted with a mono-exponential decay function decreased from 1,021 to 793 ns for the control and IPA treated films, respectively. The PL intensity (and FWHM) is observed to gradually recover with time, possibly due to trap-filling by photo-generated carriers,[17] as also seen in the control film without treatment (**Figure S3c, 3d**).

We further investigated the distribution and nature of the generated defects using Positron Annihilation Spectroscopy (PAS). Positrons are implanted from the film surface and annihilate with

electrons after trapping at negatively charged (or neutral) defects to emit two gamma photons. The incident kinetic energy is controlled to vary the positron implantation depth (**Figure 1d, Figure S4**), from which the depth-resolved defect density of the film can be investigated. The treated film had a higher Shape parameter within ~40 nm from the film surface, implying the generation of negatively charged (or neutral) defects at the top surface region. We speculate that the formed defect is possibly FA vacancy (V'_{FA}), given the solubility of FAI in IPA.

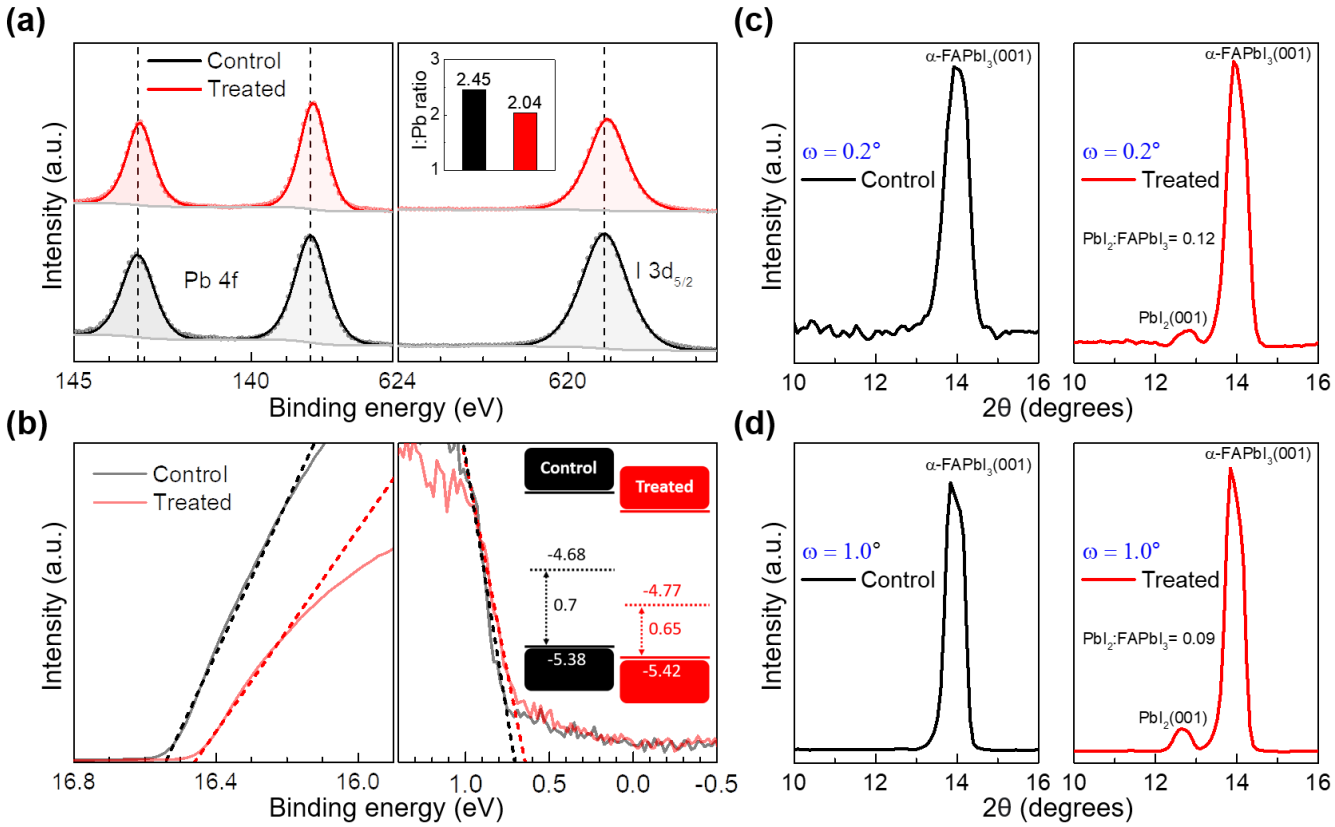

Fig. 2. Characterizations of the perovskite films. (a) High-resolution XPS spectra of the Pb 4f and I $3d_{5/2}$ peaks of the perovskite films. Inset includes the calculated I:Pb ratios of the films. Solid lines are fitted plots. Dashed vertical lines demarcate the peak positions for the control film. Intensities are normalized to Pb 4f peak. (b) UPS spectra of the perovskite films. Inset includes a schematic band diagram of the energy levels based on the UPS measurements. GIXRD diffraction patterns of the perovskite films measured with an incident angle of (c) ω = 0.2° and (d) ω = 1.0°.

The implied existence of V'_{FA} suggests that iodine vacancy ($V_I^{\bullet}$) was likely generated concurrently, but PAS is unable to ascertain this due to its insensitivity to positively charged defects (i.e. $V_I^{\bullet}$).[18,19] We therefore further probed the films with high-resolution X-ray Photoelectron Spectroscopy

(XPS). The I:Pb ratio, calculated from the integrated areas of the Pb 4f doublet and I $3d_{5/2}$ peak (**Figure 2a**), was 2.45 for the control film, and decreased to 2.04 for the treated film to approach that of stoichiometric PbI_2. We note that the ultra-high vacuum environment of the XPS instrument (~10^{-7}-10^{-8} torr) may have accelerated the outgassing of the volatile halide,[20,21] and therefore only relative comparisons would be reliable. Closer inspection of the XPS spectra further showed that all of the Pb $4f_{5/2}$ (143.19 eV to 143.13 eV), Pb $4f_{7/2}$ (138.32 eV to 138.25 eV), and I $3d_{5/2}$ (619.15 eV to 619.08 eV) characteristic peaks shifted to lower binding energies for the treated film when compared to the control, suggesting a change in the surface chemical environment. Together with the observed change in the I:Pb ratios, the shift direction and final peak positions is consistent with the formation of PbI_2 for the treated film.[22] The existence of PbI_2 was directly detected by Grazing Incidence X-ray Diffraction (XRD) at an incident angle of $\omega = 0.2°$ (penetration depth ~60 nm, see Methods for estimation) (**Figure 2c**, **2d**). Moreover, the PbI_2:$FAPbI_3$ peak intensity ratio was observed to decrease at an incident angle of $\omega = 1.0°$ (penetration depth ~310 nm), suggesting that the PbI_2 is located more towards the top perovskite region. Combining the experimental observations together, we thus propose the following reconstruction of the perovskite film surface during post-treatment, by a dissolution reaction process induced by IPA:

$$FAPbI_3\ (s) \xrightarrow{\text{IPA}} FAI\ (in\ IPA) + PbI_2\ (s) + V'_{FA} + V_I^{\bullet}$$

We now discuss some possible implications of this inferred surface reconstruction. Ultraviolet Photoelectron Spectroscopy (UPS) was used to investigate any band structure changes at the surface. The fermi level was observed to downshift from -4.68 eV for the control film to -4.77 eV for the film treated with IPA (**Figure 2b**), indicating a more p-doped surface for the latter relative to the bare perovskite surface. The overall band structure of the treated surface further downshifted relative to the vacuum level due to the deeper valence band maximum (inset of **Figure 2b**), consistent with a relatively more FAI deficient surface.[23] This possibly creates a more beneficial band bending going from the perovskite bulk to the surface contacting a hole-transporting material (**Figure S5a**). The surface PbI_2 for the treated film may additionally contribute to interfacial passivation.[24] In reality, however, we observed that the treated device performance was inferior to the control with a more pronounced current-voltage hysteresis (**Figure S5b, S5c**), likely due to the generated vacancy defects, given that defect migration (due to the bias potential) is known to underly the hysteric behavior.[4,9]

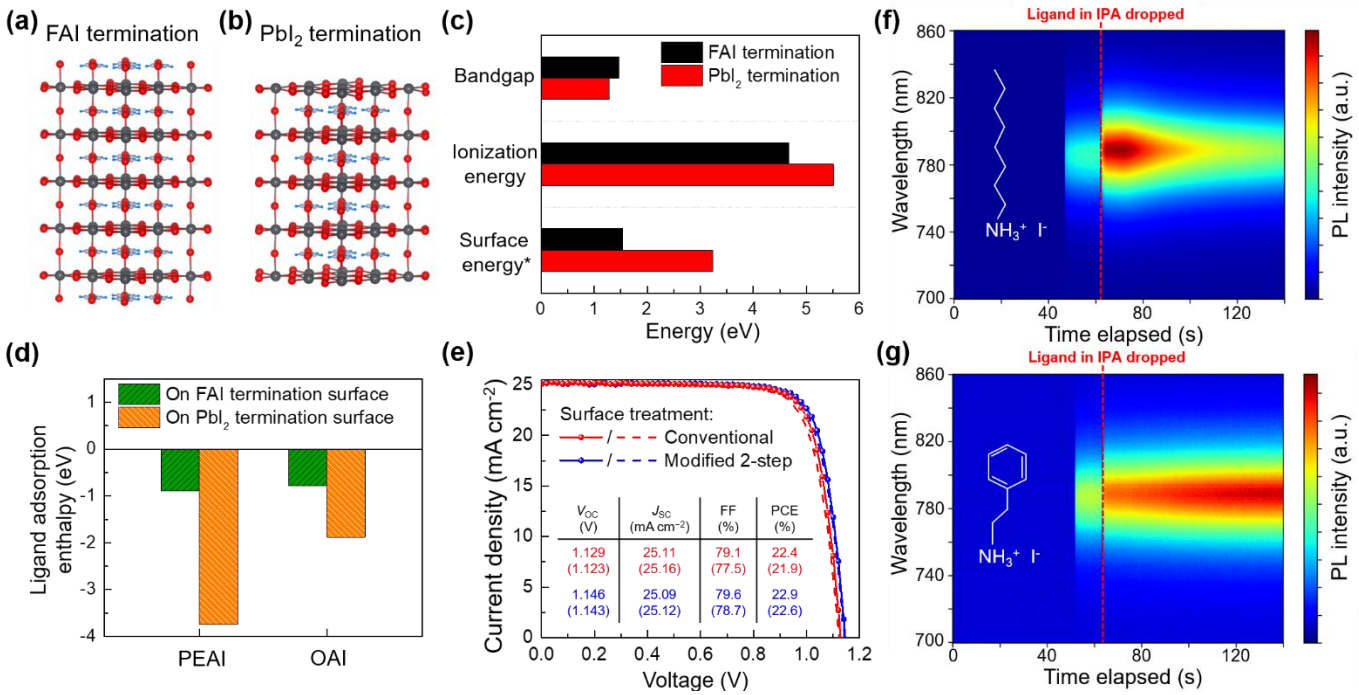

Figure 3. Surface reconstruction and its implications. (a)**,** (b) Theoretical slab models for first-principles DFT calculations. Atoms are colored black (lead), red (iodine), gray (nitrogen), and blue (hydrogen). (c) Calculated surface physiochemical properties. The asterisk indicates that surface energy is in units of eV nm^{-2}. (d) Enthalpy of adsorption of either PEAI or OAI on the surfaces. (e) Current density-voltage curves of devices treated with 10 mM OABr in CF. Inset includes the measured photovoltaic parameters. Brackets indicate parameters measured in forward bias. *In situ* PL contour plots of perovskite films undergoing surface treatment with (f) 10 mM OAI or (g) 10 mM PEAI in IPA.

First-principles density functional theory (DFT) calculations were performed on slabs based on the deduced reconstruction to compare their thermodynamics and energetics. We note that realistically, the perovskite surface is expected to be a complex amalgamation of exposed atoms, local atomic pairing/reorientation, and defected.[25] However, simplified slab models are necessarily required to reduce computational complexity. Nevertheless, *relative* comparisons can be made based on the predicted results. Experimental investigations have observed that the pristine perovskite surface (without treatment) is terminated mostly by organic halides,[26,27] which is also supported by computational results.[28] Our results imply that IPA reconstructs the surface towards a *relatively more* PbI_2-rich surface. We chose the two extreme cases of complete FAI termination (**Figure 3a**) and PbI_2 termination (**Figure 3b**) to model the pristine (control) and reconstructed (treated) surfaces, respectively, again noting that the models are used to predict *relative trends*.

The predicted bandgap decreased while the ionization energy increased for the PbI_2 termination surface (**Figure 3c**), matching the *in situ* PL and UPS observations discussed. The surface energy more than doubled (1.54 to 3.24 eV nm^{-2}) for the PbI_2 termination surface, indicating that the surface became more thermodynamically unstable with treatment. This likely contributed to the observed aggravated instability of the treated films (**Figure S6**). The generated defects might additionally lower the $FAPbI_3$ cubic-to-hexagonal phase transformation activation energy barrier to also accelerate the degradation.[29] Given the increased surface energy, we postulated that organic ammonium salts may preferentially adsorb onto the treated surface. We further calculated the formation enthalpy to attach the widely used passivation agents OAI or PEAI to the surfaces (**Figure 3d**). The adsorption enthalpies for both were significantly more negative on the PbI_2 termination surface – for OAI, -0.78 versus -1.88 eV (141% increase), and -0.9 versus -3.75 eV for PEAI (317% increase), suggesting that the surface reconstruction plays a vital role in the passivation process.

The more negative adsorption enthalpies imply that ammonium salts are thermodynamically more favored to adsorb onto the treated surface. We investigated this with a modified 2-step surface post-treatment process (**Figure S7**). Initially treating a perovskite film with pure IPA before subsequently depositing octylammonium bromide (OABr) in CF (at the same concentration) further improved the device photovoltaic performance (**Figure 3e**). The champion device surface treated with the modified 2-step approach reached a power conversion efficiency of 22.9 % in reverse bias (**Figure 3e**) with negligible current-voltage hysteresis, relative to the 22.4 % of the conventionally treated device. The improved performance was attributed to increases in the device open-circuit voltage (1.129 V to 1.146 V) and fill factor (79.1 % to 79.6 %), which is indicative of an enhanced defect passivation effect with the modified 2-step treatment. Therefore, the observations support the theoretical predictions that IPA assists in the adsorption process of ammonium salts to the surface and thus the passivation of defects. The surface is first reconstructed by removing FAI to expose the undercoordinated Pb^{2+} (i.e. $V_I^{\bullet}$) for the ammonium groups to bond with by electrostatic coulomb interactions and/or hydrogen bonding.

We speculated that the PL evolution as OAI or PEAI (in IPA) is deposited on the surface may be related to their adsorption enthalpies. Further measurements show that although both treatments led to instantaneous PL enhancements immediately upon deposition (**Figure 3f, 3g, Figure S8**), the PL intensity subsequently decayed ~10 s after deposition only for the OAI treated film. With the PbI_2 termination surface, the computed adsorption enthalpies imply a significantly weaker interaction of OAI (relative to PEAI) with the perovskite surface, which may possibly be correlated with the differing PL

dynamics. On the other hand, the adsorption enthalpies are negligibly different when calculated using the FAI termination surface, which may be challenging to reconcile with the experimental observation. We also monitored the recombination dynamics with further *in situ* PL measurements during annealing (**Figure S9a, S9b**). A rapid initial exponential decay in PL intensity was observed for both films due to increased phonon scattering at elevated temperatures.[10,12] However, only the OAI treated film counteracted the initial drop to eventually increase its PL intensity due to the activated defect passivation effect. The evolution and emission characteristics of the wide bandgap phases notably differ between the OAI and PEAI treated films, and will be the subject of future investigations (**Figure S9c, S9d, S9e**).

In summary, we observed a reconstruction of the perovskite top surface induced by IPA, which is ubiquitously used as the solvent for surface treatment with organic ammonium salts. We discussed several implications of this reconstruction on the perovskite surface energetics and thermodynamics. Importantly, given the profound differences between the reconstructed surface and the perovskite bulk/pristine surface, these results will guide further experimental and theoretical investigations of the perovskite surface and surface passivation strategies.

ASSOCIATED CONTENT

Supporting Information

The Supporting Information is available free of charge on the ACS Publications website at DOI: XXX

Materials and methods; Photographs of ammonium salts in CF; PL penetration depth estimation; *In situ* and time-resolved PL spectra of the perovskite films; PAS profile of the perovskite films; Device energy alignment and performance; Humidity stability testing on the perovskite films; Modified surface treatment process; *In situ* PL of films undergoing surface treatment; *In situ* PL of films undergoing post-annealing. (PDF)

AUTHOR INFORMATION

Corresponding Authors

Jin-Wook Lee – *SKKU Advanced Institute of Nanotechnology (SAINT) and Department of Nanoengineering, Sungkyunkwan University, Suwon 16419, Republic of Korea;*
Email: jw.lee@skku.edu

Carolin M. Sutter-Fella – *Chemical Sciences Division and Molecular Foundry, Lawrence Berkeley National Laboratory, Berkeley, California 94720, United States;*
Email: csutterfella@lbl.gov

Yang Yang – *Department of Materials Science and Engineering and California NanoSystems Institute, University of California Los Angeles, Los Angeles, California 90095, United States;*
Email: yangy@ucla.edu

Author Contributions

‡These authors contributed equally.

Notes

The authors declare no competing financial interests.

ACKNOWLEDGMENT

This work was supported by the U.S. Department of Energy's Office of Energy Efficiency and Renewable Energy (EERE) under the Solar Energy Technologies Office under award number DE-EE0008751. Dr. Carolin M. Sutter-Fella acknowledges the Molecular Foundry supported by the Department of Energy, Office of Science, Office of Basic Energy Sciences, Scientific User Facilities Division of the U.S. Department of Energy under contract no. DE-AC02-05CH11231. Dr. Marc H. Weber would like to acknowledge the detailed discussions with the late Kelvin G. Lynn. Dr. Marc H. Weber's contributions and the positron annihilation spectroscopy work was supported by subcontract to Washington State University from the University of California, Los Angeles of a grant by the U.S. Department of Energy's Office of Energy Efficiency and Renewable Energy (EERE) under the Solar Energy Technologies Office under award number DE-EE0008751 awarded to Dr. Yang Yang. Computing resources used in this work were provided by the National Center for High-Performance Computing of Turkey (UHEM) with grant number 1008342020. Dr. Ilhan Yavuz acknowledges support by the Scientific and Technological Research Council of Turkey (TÜBITAK), Grant no: 119F380. Dr. Jin-Wook Lee acknowledges support by the National Research Foundation of Korea (NRF) grant funded by the Korea government (MIST) under contract number NRF-2020R1F1A1067223. Shaun Tan, Tianyi Huang, Dr. Maged Abdelsamie, Dr. Finn Babbe, and Dr. Carolin M. Sutter-Fella acknowledge support from the Laboratory Directed Research and Development (LDRD) program of Lawrence Berkeley National Laboratory under U.S. Department of Energy contract number DE-AC02-05CH11231.

References

1. Best Research-Cell Efficiency Chart (2020). NREL.
2. Jiang, Q., Zhao, Y., Zhang, X., Yang, X., Chen, Y., Chu, Z., Ye, Q., Li, X., Yin, Z., and You, J. (2019). Surface passivation of perovskite film for efficient solar cells. Nat. Photonics *13*, 460–466.

3. Kim, G., Min, H., Lee, K.S., Lee, D.Y., Yoon, S.M., and Seok, S. Il (2020). Impact of strain relaxation on performance of α-formamidinium lead iodide perovskite solar cells. Science *370*, 108–112.
4. Tan, S., Yavuz, I., De Marco, N., Huang, T., Lee, S., Choi, C.S., Wang, M., Nuryyeva, S., Wang, R., Zhao, Y., et al. (2020). Steric Impediment of Ion Migration Contributes to Improved Operational Stability of Perovskite Solar Cells. Adv. Mater. *32*, 1906995.
5. Ball, J.M., and Petrozza, A. (2016). Defects in perovskite-halides and their effects in solar cells. Nat. Energy *1*, 1–13.
6. Lee, J.-W., Kim, S.-G., Yang, J.-M., Yang, Y., and Park, N.-G. (2019). Verification and mitigation of ion migration in perovskite solar cells. APL Mater. *7*, 1–12.
7. Ni, Z., Bao, C., Liu, Y., Jiang, Q., Wu, W.-Q., Chen, S., Dai, X., Chen, B., Hartweg, B., Yu, Z., et al. (2020). Resolving spatial and energetic distributions of trap states in metal halide perovskite solar cells. Science *367*, 1352–1358.
8. Yang, Y., Yang, M., Moore, D.T., Yan, Y., Miller, E.M., Zhu, K., and Beard, M.C. (2017). Top and bottom surfaces limit carrier lifetime in lead iodide perovskite film. Nat. Energy *2*, 1–7.
9. Han, T.-H., Tan, S., Xue, J., Meng, L., Lee, J.-W., and Yang, Y. (2019). Interface and Defect Engineering for Metal Halide Perovskite Optoelectronic Devices. Adv. Mater. *31*, 1803515.
10. Babbe, F., and Sutter-Fella, C.M. (2020). Optical Absorption-Based In Situ Characterization of Halide Perovskites. Adv. Energy Mater. *10*, 1903587.
11. Song, T.-B., Yuan, Z., Babbe, F., Nenon, D.P., Aydin, E., De Wolf, S., and Sutter-Fella, C.M. (2020). Dynamics of Antisolvent Processed Hybrid Metal Halide Perovskites Studied by In Situ Photoluminescence and Its Influence on Optoelectronic Properties. ACS Appl. Energy Mater. *3*, 2386–2393.
12. Song, T., Yuan, Z., Mori, M., Motiwala, F., Segev, G., Masquelier, E., Stan, C. V., Slack, J.L., Tamura, N., and Sutter-Fella, C.M. (2020). Revealing the Dynamics of Hybrid Metal Halide Perovskite Formation via Multimodal In Situ Probes. Adv. Funct. Mater. *30*, 1908337.
13. Lee, J.-W., Tan, S., Han, T.-H., Wang, R., Zhang, L., Park, C., Yoon, M., Choi, C., Xu, M., Liao, M.E., et al. (2020). Solid-phase hetero epitaxial growth of α-phase formamidinium perovskite. Nat. Commun. *11*, 5514.
14. Prochowicz, D., Tavakoli, M.M., Solanki, A., Goh, T.W., Pandey, K., Sum, T.C., Saliba, M., and Yadav, P. (2018). Understanding the effect of chlorobenzene and isopropanol anti-solvent

treatments on the recombination and interfacial charge accumulation in efficient planar perovskite solar cells. J. Mater. Chem. A *6*, 14307–14314.

15. Wang, X., Li, X., Tang, G., Zhao, L., Zhang, W., Jiu, T., and Fang, J. (2015). Improving efficiency of planar hybrid CH3NH3PbI3-xClx perovskite solar cells by isopropanol solvent treatment. Org. Electron. *24*, 205–211.
16. Yoo, J.J., Wieghold, S., Sponseller, M.C., Chua, M.R., Bertram, S.N., Putri, T., Tresback, J.S., Hansen, E.C., Correa-Baena, J.-P., Bulović, V., et al. (2019). An interface stabilized perovskite solar cell with high stabilized efficiency and low voltage loss. Energy Environ. Sci. *12*, 2192–2199.
17. DeQuilettes, D.W., Zhang, W., Burlakov, V.M., Graham, D.J., Leijtens, T., Osherov, A., Bulović, V., Snaith, H.J., Ginger, D.S., and Stranks, S.D. (2016). Photo-induced halide redistribution in organic–inorganic perovskite film. Nat. Commun. *7*, 1–9.
18. Barthe, M.-F., Labrim, H., Gentils, A., Desgardin, P., Corbel, C., Esnouf, S., and Piron, J.P. (2007). Positron annihilation characteristics in UO2: for lattice and vacancy defects induced by electron irradiation. Phys. Status Solidi C *10*, 3627–3632.
19. Wiktor, J., Jomard, G., Torrent, M., and Bertolus, M. (2017). First-principles calculations of momentum distributions of annihilating electron–positron pairs in defects in UO2. J. Phys. Condens. Matter *29*, 1–9.
20. Jiang, Y., Yang, S.-C., Jeangros, Q., Pisoni, S., Moser, T., Buecheler, S., Tiwari, A.N., and Fu, F. (2020). Mitigation of Vacuum and Illumination-Induced Degradation in Perovskite Solar Cells by Structure Engineering. Joule *4*, 1087–1103.
21. Das, C., Wussler, M., Hellmann, T., Mayer, T., and Jaegermann, W. (2018). In situ XPS study of the surface chemistry of MAPI solar cells under operating conditions in vacuum. Phys. Chem. Chem. Phys. *20*, 17180–17187.
22. Juarez-Perez, E.J., Ono, L.K., Maeda, M., Jiang, Y., Hawash, Z., and Qi, Y. (2018). Photodecomposition and thermal decomposition in methylammonium halide lead perovskites and inferred design principles to increase photovoltaic device stability. J. Mater. Chem. A *6*, 9604–9612.
23. Meggiolaro, D., Mosconi, E., Proppe, A.H., Quintero-Bermudez, R., Kelley, S.O., Sargent, E.H., and De Angelis, F. (2019). Energy Level Tuning at the MAPbI3 Perovskite/Contact Interface Using Chemical Treatment. ACS Energy Lett. *4*, 2181–2184.

24. Chen, Q., Zhou, H., Song, T. Bin, Luo, S., Hong, Z., Duan, H.S., Dou, L., Liu, Y., and Yang, Y. (2014). Controllable self-induced passivation of hybrid lead iodide perovskites toward high performance solar cells. Nano Lett. *14*, 4158–4163.

25. Leblebici, S.Y., Leppert, L., Li, Y., Reyes-Lillo, S.E., Wickenburg, S., Wong, E., Lee, J., Melli, M., Ziegler, D., Angell, D.K., et al. (2016). Facet-dependent photovoltaic efficiency variations in single grains of hybrid halide perovskite. Nat. Energy *1*, 1–7.

26. She, L., Liu, M., and Zhong, D. (2016). Atomic structures of CH3NH3PbI3 (001) surfaces. ACS Nano *10*, 1126–1131.

27. Stecker, C., Liu, K., Hieulle, J., Ohmann, R., Liu, Z., Ono, L.K., Wang, G., and Qi, Y. (2019). Surface Defect Dynamics in Organic− Inorganic Hybrid Perovskites: From Mechanism to Interfacial Properties. ACS Nano *13*, 12127–12136.

28. Geng, W., Tong, C.-J., Tang, Z.-K., Yam, C., Zhang, Y.-N., Lau, W.-M., and Liu, L.-M. (2015). Effect of surface composition on electronic properties of methylammonium lead iodide perovskite. J. Mater. *1*, 213–220.

29. Tan, S., Yavuz, I., Weber, M.H., Huang, T., Chen, C.-H., Wang, R., Wang, H.-C., Ko, J.H., Nuryyeva, S., Xue, J., et al. (2020). Shallow Iodine Defects Accelerate the Degradation of α-Phase Formamidinium Perovskite. Joule *4*, 2426–2442.